Published in final edited form as:
*Circ Res*. 2014 February 14; 114(4): 650–659. doi:10.1161/CIRCRESAHA.114.302884.

# Preclinical Evaluation of the Engineered Stem Cell Chemokine Stromal Cell-Derived Factor 1–alpha Analogue in a Translational Ovine Myocardial Infarction Model

**John W. MacArthur Jr**[1,2], **Jeffrey E. Cohen**[1,2], **Jeremy R. McGarvey**[1,3], **Yasuhiro Shudo**[1], **Jay B. Patel**[2], **Alen Trubelja**[1], **Alexander S. Fairman**[1], **Bryan B. Edwards**[1], **George Hung**[1], **William Hiesinger**[1], **Andrew B. Goldstone**[1], **Pavan Atluri**[1], **Robert L. Wilensky**[4], **James J. Pilla**[3,5], **Joseph H. Gorman III**[1,3], **Robert C. Gorman**[1,3], and **Y. Joseph Woo**[1]

[1]Division of Cardiovascular Surgery, Department of Surgery, University of Pennsylvania School of Medicine, Philadelphia, PA 19104

[2]Department of Cardiothoracic Surgery, Stanford University School of Medicine, Stanford, CA 94305

[3]Gorman Cardiovascular Research Group, Department of Surgery, University of Pennsylvania School of Medicine, Philadelphia, PA 19104

[4]Division of Interventional Cardiology,. Department of Medicine, University of Pennsylvania School of Medicine, Philadelphia, PA 19104

[5]Department of Radiology, University of Pennsylvania School of Medicine, Philadelphia, PA 19104

## Abstract

**Rationale—**Following myocardial infarction (MI) there is an inadequate blood supply to the myocardium and the surrounding borderzone becomes hypocontractile.

**Objective—**To develop a clinically translatable therapy, we hypothesized that in a preclinical ovine model of MI, the modified endothelial progenitor stem cell (EPC) chemokine, engineered stromal cell-derived factor 1-alpha analogue (ESA), would induce EPC chemotaxis, limit adverse ventricular remodeling, and preserve borderzone contractility.

**Methods and Results—**Thirty six adult male Dorset sheep underwent permanent ligation of the left anterior descending coronary artery, inducing an anteroapical infarction and were randomized to borderzone injection of saline (n=18) or ESA (n=18). Ventricular function, geometry, and regional strain were assessed using cardiac magnetic resonance imaging and pressure-volume catheter transduction. Bone marrow was harvested for in-vitro analysis, and myocardial biopsies were taken for mRNA, protein and immunohistochemical analysis. ESA induced greater chemotaxis of EPCs compared to saline ($p<0.01$), and was equivalent to recombinant stromal cell-derived factor 1-alpha ($p=0.27$). Analysis of mRNA expression and

Address correspondence to: Dr. Y. Joseph Woo, Department of Cardiothoracic Surgery, Stanford University, Falk Cardiovascular Research Bldg, 2nd Floor, 300 Pasteur Drive, Stanford CA 94305-5407, Tel: (650)-725-3828.

**Disclosures:** None

protein levels in ESA treated animals revealed reduced MMP-2 in the borderzone ($p<0.05$), with elevated levels of TIMP-1 and elastin in the infarct ($p<0.05$), while immunohistochemical analysis of borderzone myocardium showed increased capillary and arteriolar density in the ESA group ($p<0.01$). Animals in the ESA treatment group also had significant reductions in infarct size ($p<0.01$), increased maximal principle strain in the borderzone ($p<0.01$), and a steeper slope of the end systolic pressure volume relationship ($p=0.01$).

**Conclusions—**The novel, biomolecularly-designed peptide ESA induces chemotaxis of EPCs, stimulates neovasculogenesis, limits infarct expansion, and preserves contractility in an ovine model of MI.

### Keywords

Endothelial progenitor cells; cardiac MRI; ventricular wall stress; reverse remodeling

## Introduction

Heart disease is the cause of significant morbidity and mortality in the US with estimates of nearly 800,000 new acute coronary events each year and accounts for a substantial proportion of the national health care expenditure.[1, 2] The cellular events following a myocardial infarction (MI) result in inadequate microvascular perfusion which causes a change in the composition of the extracellular matrix (ECM) with regional alterations in levels of matrix metalloproteinase (MMP) and tissue inhibitors of metalloproteinase (TIMP). These pathophysiologic changes result in hypocontractile scar formation, myocyte apoptosis, and progressive ventricular dilatation.[3] The differential MMP/TIMP ratio leads to deleterious remodeling from proteolytic degradation of the ECM occurring over time. This increases the stress-strain relationship of ventricular myocytes and leads to inefficient contractility, infarct spreading and ultimately heart failure.[4-9] When current treatments for coronary artery disease fail, they usually do so because microvascular perfusion is not adequately restored – a critical, independent predictor of ventricular remodeling, reinfarction, heart failure, and death.[10]

Inadequate microvascular perfusion also plays an important role in the progression to heart failure after MI.[10] To this end, many groups have experimented with various cell delivery and cytokine treatment regimens in an attempt to stimulate angiogenesis, with varying degrees of success.[11-14] One such cytokine, stromal cell-derived factor 1-alpha (SDF-1), is a key regulator in hematopoietic stem cell trafficking between the bone marrow and peripheral circulation and effectively localizes endothelial progenitor cells (EPCs) to areas of ischemia.[15-18] SDF-1 is part of the C-X-C chemokine family, causing stem cell migration through interaction with the seven transmembrane domain G protein coupled receptor CXCR 4. Following MI, cardiac secretion of SDF-1 is insufficiently robust to mobilize a sufficient population of EPCs to affect meaningful changes in perfusion. However, supraphysiologic doses of intramyocardial SDF-1 have been shown by our group and others to increase vasculogenesis, decrease cardiac myocyte apoptosis, increase cardiac myocyte survival, and preserve ventricular geometry.[19-25]

Despite the reported beneficial effects of recombinant SDF-1 after an ischemic insult, it has some limitations. SDF-1 is broken down by multiple peptidases (CD26/DPP-IV) and requires *Escherichia coli* for production, a process that is inefficient and expensive. Recently, we have designed a biochemically modified, synthetic version of SDF-1 which we named ESA in order to overcome these hurdles, and have shown it to be effective in a small animal model of MI.[26-31] In the current study, we hypothesized that intramyocardial delivery of ESA in a translational ovine model of MI would result in chemotaxis of EPCs, increased microrevascularization, limited ventricular remodeling, and improved regional and global ventricular function.

## Methods

All experiments pertaining to this investigation conformed to the "Guide for the Care and Use of Laboratory Animals," published by the US National Institutes of Health (Eighth Edition, 2011). The protocol was approved by the Institutional Animal Use and Care Committee of the University of Pennsylvania (protocol number 803430).

### Custom peptide synthesis

We have previously reported on the design and synthesis of an engineered SDF-1 peptide analogue - ESA.[27] Briefly, in order to minimize the profile of the peptide, the CXCR4 receptor binding N-terminus and the molecular stabilizing C-terminus were preserved while the central beta pleated sheet was deleted. Using computational modeling, it was determined that a 2 proline residue "linker" joining this modified sequence would durably retain a three-dimensional protein configuration similar to the native SDF-1 (Online figure I). The engineered protein was then synthesized using solid phase peptide synthesis, where the N α-amino acids are incorporated into the peptide in a step-wise fashion while one end is attached to a solid support matrix.

### Endothelial progenitor cell chemotaxis

Bone marrow mononuclear cells were isolated from the long bones of adult male Dorset sheep by density centrifugation with Histopaque 1083 (Sigma-Aldrich), plated on vitronectin coated dishes, and cultured in endothelial basal medium-2 supplemented with EGM-2 SingleQuot (Lonza) containing human epidermal growth factor, FBS, vascular endothelial growth factor, basic human fibroblast growth factor, recombinant human long R3 insulin-like growth factor-1, ascorbic acid, heparin, gentamicin, and amphotericin-B. Media was changed on culture day 4 and non-adherent bone marrow mononuclear cells were discarded, enriching for the EPC phenotype. A modified transwell migration assay (Boyden Chamber, Neuro Probe, Gaithersburg, MD) was used to assess EPC migration as previously described.[23, 26, 27]

(See Online Data Supplement for a detailed description).

### Animal model

Myocardial infarction was induced in 36 adult male Dorset sheep (weighing between 35-45 kg) using an established and highly reproducible model.[32] Briefly, the animals were induced

with IM midazolam (0.4mg/kg) and ketamine (5mg/kg) and anesthesia was maintained on inhaled isoflurane (1.5-3%). An anterior, 5 cm mini-thoracotomy was utilized to access the chest cavity and the heart was exposed. The distal left anterior descending and the second diagonal coronary arteries were ligated with a 4-0 polypropylene suture, creating an anteroapical area of ischemia (Figure 1). Animals were randomized to receive either 1ml of saline (n=18), or 6μg/kg of ESA (n=18) diluted in 1ml of saline, injected via a custom made 25-gauge end capped needle (Cadence Inc, Staunton VA) with three side holes each separated by 120 degrees, in 10 equal aliquots around the borderzone of the ischemic myocardium. The concentration of ESA administered was chosen based on dose response curves we have previously published on.[26, 29] Continuous ECG monitoring was employed throughout the procedure. All animals received an intramuscular injection of sargramostim (granulocyte-macrophage colony stimulating factor, 40μg/kg). Animals were recovered from anesthesia and buprenorphine (0.05mg/kg) IM along with a transdermal fentanyl patch (75μg/hr) were used for postoperative pain control. A total of 5 animals developed refractory ventricular fibrillation immediately after ligation (n=3 in the saline group, n=2 in the ESA group), and one animal in the saline group died during the follow up period (autopsy revealed intestinal volvulus with resultant perforation). All surviving animals were euthanized 8 weeks after MI.

### Cardiac magnetic resonance imaging

A subset of animals (ESA, n=7; saline, n=5) underwent cardiac MRI before and 8 weeks following MI to assess global ventricular function, ventricular geometry, and 3D strain. General anesthesia was maintained for the entirety of the imaging procedures, as described above. A high-fidelity pressure transduction catheter (Millar Instruments; Houston, TX) was inserted into the left ventricle (LV) via the carotid artery under fluoroscopic guidance for LV pressure gating during image acquisition. MRI was performed using a 3T MAGNETOM Verio scanner (Seimens; Malvern, PA) before infarction and 8 weeks after infarction as previously described.[33]

(See Online Data Supplement for a detailed description and Online Video I for representative long axis cine loops).

### MRI image post-processing

Treatment groups of the imaging data sets were blinded to the end-user throughout post-processing. LV volume and global function data were obtained using prospective steady state free precession (SSFP) cine MRI images. Raw short-axis images were automatically sorted, cropped, and contrast normalized in a custom Matlab (Natick, MA) program to ensure homogenous LV coverage and image quality, respectively. Segmentation was then performed through all cardiac phases of the sorted and correct images using a semi-automated 3D active contour segmentation program (ITK-SNAP, open access/source).[34] LV end-diastolic volume (EDV), end-systolic volume (ESV), stroke volume (SV), and ejection fraction (EF) were then computed throughout the entire cardiac cycle from segmented images using in-plane and through-plane spatial resolution information.

Systolic regional strain measurements from the borderzone were calculated from 3D spatial modulation of magnetization (SPAMM) acquisitions using an optical flow technique as previously described (Figure 2).[35] Maximum principle strain ($\varepsilon_1$) was then calculated for each region and 3D strain maps were generated.

(See Online Data Supplement for a detailed description).

### Invasive hemodynamic assessment

Pressure volume (PV) loops were acquired in all animals before infarction and 8 weeks following MI. A ventri-cath PV catheter transducer (Millar Instruments Inc, Houston, TX) was placed into the LV via the right carotid artery. Steady state PV loops were acquired during a 10 second breath hold, followed by IVC occlusion in order to produce static and dynamic loops under varying load conditions. Coronary angiograms were performed and cardiac output was measured using peri-aortic Doppler flow probes (Transonic Systems, Ithaca NY).

(See Online Data Supplement for a detailed description and Online Video II for a representative coronary angiogram).

### Histologic analysis and immunohistochemistry

In order to assess ventricular geometry, infarct size, and microvascular angiogenesis, hearts were explanted after the invasive hemodynamic assessment was performed and flushed with saline. The atria were removed and the left ventricle opened along the posterior septum. Standardized digital photographs were taken with a Nikon D5100 SLR camera (Nikon, Tokyo, Japan). Photographs were uploaded to ImageJ (v1.46b) and the size of the infarct assessed with digital planimetry. Ventricular samples (3 $cm^3$) were taken from the infarct, borderzone, and remote myocardium, snap frozen in liquid nitrogen, and stored in a -80°C freezer. 10μm thick sections were prepared from each biopsy specimen.

10μm thick sections from the borderzone of each heart were stained with antibodies directed against von Willebrand Factor (vWF) and separately for alpha smooth muscle actin (αSMA) in order to quantify capillary and arteriolar density, as previously described.[31]

### Ventricular extracellular matrix mRNA profiling

RNA was isolated from frozen myocardium using a QuantiGene Sample Processing kit (Affymetrix) according to the manufacturer's instructions. mRNA was analyzed with a matrix metalloproteinase profile (1,2,7,8,9,12,14), tissue inhibitor of matrix metalloproteinase profile (1,2,4), elastin, and transforming growth factor beta using QuantiGene 2.0 Plex Assay kit (Affymetrix) according to the manufacturer's protocol.

(See Online Data Supplement for detailed description).

### Ventricular extracellular matrix protein expression

LV myocardial biopsies (10$mm^3$) were removed from the LV at the time of explant (regions: infarct, borderzone, and remote) and snap frozen in liquid nitrogen. Samples were homogenized in T-PER protein extraction reagent along with HALT protease inhibitor

(Thermo Scientific, Waltham MA). Final protein concentrations were determined using the Qubit protein assay (Qubit fluorimeter, Life Technologies, Carlsbad CA). The extracellular membrane profile of each myocardial region was assessed via immunoblotting.

(See Online Data Supplement for further details including specific antibodies used).

### Statistical analysis

All analyzed variables approximated a normal distribution, and values for continuous variables were reported as means ± standard deviation. A 1-way ANOVA with Tukey correction was used for comparison of continuous variables between groups. Statistical significance was set at p less than 0.05. Analyses were performed with STATA (StataCorp, College Station, TX) statistical software package, version 12.1.

## Results

### ESA induces chemotaxis of sheep EPCs

In order to confirm the efficacy of ESA in sheep, a transwell migration assay was utilized. EPCs showed significantly increased chemotaxis towards ESA compared to saline alone (saline, 97.3 EPCs/ $mm^2$ ± 4.9; ESA, 611 EPCs/ $mm^2$ ± 21.7; $p<0.01$), indicating that the custom peptide actively binds to sheep EPCs. Importantly, the degree of EPC chemotaxis was similar between the ESA and the recombinant SDF-1 groups (SDF, 568 EPCs/ $mm^2$ ± 37.5; ESA, 611 EPCs/ $mm^2$ ± 21.7; $p=0.27$) (Figure 3).

### Differential ventricular ECM mRNA expression and protein concentration

Biopsies from the infarct, borderzone, and remote myocardium were taken for RNA analysis and assessed for MMP, TIMP, elastin, and TGFβ levels. RNA levels of MMP-2 were found to be elevated in the borderzone myocardium from sheep in the saline control group compared to the ESA group (saline, 0.1 RFU ± 0.01; ESA, 0.03 RFU ± 0.01; $p<0.05$) while there was no difference in the other MMPs from any myocardial region between groups. Interestingly, RNA levels of TIMP-1 and elastin were elevated in the infarct of ESA treated animals (TIMP-1; saline, 0.3 RFU ± 0.4; ESA 2.4 RFU ± 1.0; $p<0.05$, elastin; saline, 0.3 RFU ± 0.2; ESA, 3.1 RFU ± 1.2; $p<0.05$). RNA expression profiles from all regions are presented in Figure 4.

In order to determine whether the differential changes in MMP and TIMP mRNA expression between groups led to differences in protein concentration and were not undergoing alterations in post-transcriptional or post-translational modification events, immunoblots were performed. Results were consistent with the mRNA expression data, where protein levels of MMP-2 were elevated in the myocardium of sheep from the saline group compared to the ESA group (saline, 0.58 ± 0.05; ESA, 0.074 ± 0.037; $p<0.05$) with no differences in any of the other MMP protein levels between groups. Again, TIMP-1 and elastin protein concentrations were higher in the infarct region of myocardium from ESA treated animals (TIMP-1; saline, 0.38 ± 0.03; ESA, 0.73 ± 0.18; $p<0.05$, elastin; saline, 0.17 ± 0.04; ESA, 0.66 ± 0.3; $p<0.05$). There were no significant differences among the other protein levels of

myocardial regions between groups. Representative immunoblot results for MMP-2 (infarct), TIMP-1 (borderzone), and elastin (borderzone) are presented in Figure 4.

### Microvascular density and myocardial perfusion

Biopsies from the borderzone were sectioned and stained for vWF and αSMA. Analysis of immunofluorescently labeled vWF and αSMA showed a significant increase in both capillary and arteriolar density in the ESA group when compared to the saline control (vWF: saline, 7.5 capillaries/$mm^2$ ± 1.4; ESA, 17.7 capillaries/$mm^2$ ± 4.2; $p<0.01$, SMA: saline, 10.8 arterioles/$mm^2$ ± 2.6; ESA, 18.4 arterioles/$mm^2$ ± 2.7; $p<0.01$). Representative images are shown in Figure 5.

In order to determine if the increased vascularity actually improved myocardial perfusion, coronary angiograms were performed and assessed for collateral filling using a previously validated method described by Rentrop et al.[36] Rentrop scores were calculated for each animal and averaged for each group. The saline group had significantly less collateral filling when compared to the ESA group (saline, 0.5 ± 0.7; ESA, 2.0 ± 0.8; $p<0.05$).

(See Online Video II for a representative coronary angiogram).

### ESA treatment improves regional strain and lv function, while limiting remodeling

Maximal principle strain ($\varepsilon_1$) was measured in the borderzone region of animals treated with ESA and saline before and 8 weeks following MI. $\varepsilon_1$ is indicative of radial myocardial displacement, and the magnitude of in-plane displacement was depicted as a color map overlay (Figure 6). Late gadolinium enhanced (LGE) images were used for infarct identification and aided in choosing the appropriate regions of interest within the strain color maps. The composite strain data show that animals treated with ESA had significantly elevated $\varepsilon_1$ within the borderzone compared to saline control (saline, 8.8% ± 3.3; ESA, 12.4% ± 5.8; $p<0.01$), indicative of differential systolic stretching and radial wall thickening between groups. Because radial strain was measured, changes in the thickness of borderzone myocardium between systole and diastole could be evaluated – measures which correlate to regional contractility. Thus, the increased borderzone strain seen in hearts from animals in the ESA group is a result of improved and more efficient myocardial contraction compared to hearts from animals in the saline group.

Steady-state free precession (SSFP) cine MRI images were used to calculate EF, SV, ESV, and EDV for both treatment groups. At baseline, the EF was 46%, similar to previous studies using Dorset sheep.[37, 38] Eight weeks after infarction, animals in the saline group had a decline in EF to 27.8% ± 4.9 while animals in the ESA group had a relatively preserved EF of 36.4% ± 6.4 ($p=0.01$). Additionally, animals in the saline group had significantly larger ESV and EDV (ESV: saline, 96.5 ml ± 21.2; ESA, 70.4 ml ± 12.4; $p=0.01$; EDV: saline, 136.9 ml ± 22.4; ESA, 109.3 ml ± 17.5; $p<0.05$) suggestive of reduced ventricular dilatation and attenuation of LV remodeling in the ESA group (Figure 7).

LV systolic function was further assessed using a PV catheter transducer and aortic flow probe. The slope of the end systolic pressure volume relationship (ESPVR) curve was derived from PV loops during IVC occlusion and represents end systolic elastance, an

approximation of myocardial contractility (See Figure 7 for representative PV loops). Animals in the ESA group had an elevation in the slope of the ESPVR when compared to saline control (saline, 1.6 ± 0.07; ESA, 6.9 ± 2.6; p=0.01) consistent with improved LV contractility. Furthermore, cardiac output, as measured by peri-aortic flow probe assessment, was significantly higher in the ESA group compared to saline control (saline, 2.8 L/min ± 0.8; ESA, 4.1 L/min ± 1.1; p=0.01). There was no difference in heart rate between groups.

At the time of terminal surgery, after all invasive hemodynamic parameters were obtained, animals were euthanized with retrograde KCl injection, hearts were explanted, the LV was opened, and the infarct was outlined and photographed. Quantification of infarct size, measured as a percentage of total LV area, revealed a significant infarct reduction in the ESA group compared to saline group (saline, 21% ± 1.9; ESA, 14% ± 0.38; p<0.01) (Figure 8).

## Discussion

In this study, we attempted to evaluate the efficacy of intramyocardial injection of the novel engineered peptide ESA in a large animal model of MI in order to demonstrate the translational potential of this peptide. Here, we have successfully shown that ESA treatment results in effective EPC chemotaxis, increased capillary density in the borderzone, elevated borderzone maximal principle strain, reduced LV remodeling, and improved LV dynamics in post-MI sheep. This data builds upon our initial experience with ESA in small animal models of MI, where similar findings were noted.[26, 27, 30] Initially, we attempted to show that ESA retained its chemokine effect on sheep EPCs because we had previously demonstrated its efficacy only on mouse and rat EPCs. The results from the transwell migration assay quite conclusively prove the ability of ESA to induce migration of sheep EPCs. This holds significant importance when evaluating capillary and arteriolar density between the ESA and saline groups, as ESA localizes EPCs to the site of injury, initiating neovasculogenesis and creating new capillaries resulting in perfused arteriolar networks. The microrevascularization that takes place after ESA treatment allows for retention of the ECM, reduction of infarct spreading, and improved regional and global LV function.

In order to further understand the mechanism behind the attenuation of LV remodeling seen in the ESA group; we studied the transcriptional regulation of select MMPs/TIMPs by quantification of mRNA levels within different regions of the ventricle (infarct, borderzone, and remote) and further assessed myocardial samples for their protein concentrations, showing concordance between mRNA and protein expression. Other groups have clearly shown that MMPs are upregulated in the infarct and borderzone after MI (specifically MMP 1,2,13, and 14) while TIMPs are downregulated (specifically TIMP 1,2, and 4) when compared to levels found in normal myocardium.[6-8] This regional and type specific alteration in the MMP/TIMP expression profile leads to dysfunctional alteration in LV geometry due to ECM breakdown and infarct expansion. Our findings of decreased expression of MMP-2 within the borderzone and increased expression of TIMP-1 within the infarct of ESA treated animals compared to saline control, provides causal support for the decreased infarct size and limited LV remodeling seen within the ESA group. We believe that the chemotactic properties of ESA localizes endothelial progenitor cells to and around

the infarct, causing microrevascularization, leading to preservation of the ECM and differential expression of MMPs and TIMPs, respectively. This theoretical explanation is supported by a study showing increased TIMP-1 and TIMP-2 levels *in vitro* from secretion by CD34+ bone marrow progenitor cells.[39] It is also worth mentioning that elastin mRNA and protein levels within infarcted tissue were statistically higher in the ESA group, an additional finding that supports maintenance of ECM within the infarct. The benefits of increased elastin levels within an infarct, such as decreased remodeling and improvement in LV hemodynamics, have been published by multiple different groups.[40, 41]

A key innovation in the current study was the application of highly advanced post-processing software for the calculation of regional strain relying on sophisticated 3D cardiac MRI tissue tagging technology using a 3D optical flow technique. This externally validated method has proven enormously useful in the ability to accurately assess myocardial strain *in vivo*, and with excellent in-plane and through-plane resolution, accurate quantification of regional strain is possible. Our results of increased regional strain in the borderzone of ESA treated animals suggests that myocardium in this region is thicker at end-systole, which may be indicative of improved regional contractility. This is an intriguing finding, and one that we have hypothesized in the past but until now have been unable to definitively prove.[30] With improved borderzone strain, ESA treated animals exhibited improved global LV contractility with significant increases in the slope of the ESPVR along with greatly improved cardiac output. The improvements seen in LV function are likely multifactorial, and begin with improved borderzone vascularity, which leads to limited expansion of the infarct and decreased LV remodeling. The preservation of regional strain within the borderzone and its effect on global LV function has important clinical implications for the use of ESA in the prevention of ischemic cardiomyopathy in patients with acute MI.

## Limitations

One limitation of this study is that it was performed in an acute animal model of MI, where the treatment was given immediately after coronary artery ligation. Although this satisfies our question for how ESA interacts with bone marrow progenitor cells and the effects these cells have on the myocardium, the positive findings reported here may not be extrapolated to include the breadth of pathology seen in human subjects, as often times treatment modalities must be effective in the setting of chronic heart failure. Chronic post-ischemic changes in a typical patient with ischemic cardiomyopathy offer a complex problem to the investigator, where deleterious remodeling has already taken place and a diminutive stem cell supply must be overcome. However, as a proof of principle study and a starting point, we have demonstrated here that ESA is effective in a sheep model of MI.

## Conclusions

In summary, intramyocardial injection of ESA induces chemotaxis of EPCs resulting in microrevascularization of the myocardium, increases maximal principle strain in the borderzone, limits ventricular remodeling, and improves ventricular function. The findings presented here illustrate the efficacy of ESA therapy post-MI and provide substantial support for the translational potential of this novel peptide in the treatment of heart disease.

## Supplementary Material

Refer to Web version on PubMed Central for supplementary material.

## Acknowledgments

We thank Jean Boyer (University of Pennsylvania Immunology core laboratory) for her help and expertise with myocardial RNA isolation and analysis and Gerald Zsido II (University of Pennsylvania, Gorman Cardiovascular Research Group) for his guidance and expert assistance with cardiac gated MRI acquisition.

**Sources of Funding:** This study was supported in part by NIH grants 1R01 HL089315-01, “Angiogenic Tissue Engineering to Limit Post-Infarction Ventricular Remodeling” (YJW); HL63954, HL73021, HL103723 (RCG, JHG); NIH training grant T32 HL007843-15 (JWM); Established Investigator Awards from the American Heart Association (RCG, JHG); Scientist Development Grant from the American Heart Association (PA); and a Post-Doctoral Fellowship Grant from the American Heart Association 12POST11620024 (JWM).

## References

1. Go AS, Mozaffarian D, Roger VL, Benjamin EJ, Berry JD, Borden WB, Bravata DM, Dai S, Ford ES, Fox CS, Franco S, Fullerton HJ, Gillespie C, Hailpern SM, Heit JA, Howard VJ, Huffman MD, Kissela BM, Kittner SJ, Lackland DT, Lichtman JH, Lisabeth LD, Magid D, Marcus GM, Marelli A, Matchar DB, McGuire DK, Mohler ER, Moy CS, Mussolino ME, Nichol G, Paynter NP, Schreiner PJ, Sorlie PD, Stein J, Turan TN, Virani SS, Wong ND, Woo D, Turner MB. American Heart Association Statistics C; Stroke Statistics S. Heart disease and stroke statistics--2013 update: A report from the american heart association. Circulation. 2013; 127:e6–e245. [PubMed: 23239837]
2. Heidenreich PA, Trogdon JG, Khavjou OA, Butler J, Dracup K, Ezekowitz MD, Finkelstein EA, Hong Y, Johnston SC, Khera A, Lloyd-Jones DM, Nelson SA, Nichol G, Orenstein D, Wilson PW, Woo YJ. American Heart Association Advocacy Coordinating C, Stroke C, Council on Cardiovascular R Intervention, Council on Clinical C, Council on E Prevention, Council on A, Thrombosis Vascular B, Council on C, Critical C, Perioperative, Resuscitation, Council on Cardiovascular N, Council on the Kidney in Cardiovascular D, Council on Cardiovascular S, Anesthesia, Interdisciplinary Council on Quality of C, Outcomes R. Forecasting the future of cardiovascular disease in the united states: A policy statement from the american heart association. Circulation. 2011; 123:933–944. [PubMed: 21262990]
3. Yankey GK, Li T, Kilic A, Cheng G, Satpute A, Savai K, Li S, Moainie SL, Prastein D, DeFillipi C, Wu ZJ, Griffith BP. Regional remodeling strain and its association with myocardial apoptosis after myocardial infarction in an ovine model. The Journal of thoracic and cardiovascular surgery. 2008; 135:991–998. 998 e991-992. [PubMed: 18455574]
4. Jackson BM, Gorman JH, Moainie SL, Guy TS, Narula N, Narula J, John-Sutton MG, Edmunds LH Jr, Gorman RC. Extension of borderzone myocardium in postinfarction dilated cardiomyopathy. Journal of the American College of Cardiology. 2002; 40:1160–1167. discussion 1168-1171. [PubMed: 12354444]
5. Jayasankar V, Woo YJ, Bish LT, Pirolli TJ, Berry MF, Burdick J, Bhalla RC, Sharma RV, Gardner TJ, Sweeney HL. Inhibition of matrix metalloproteinase activity by timp-1 gene transfer effectively treats ischemic cardiomyopathy. Circulation. 2004; 110:II180–186. [PubMed: 15364860]
6. Spinale FG, Koval CN, Deschamps AM, Stroud RE, Ikonomidis JS. Dynamic changes in matrix metalloprotienase activity within the human myocardial interstitium during myocardial arrest and reperfusion. Circulation. 2008; 118:S16–23. [PubMed: 18824748]
7. Dixon JA, Gorman RC, Stroud RE, Mukherjee R, Meyer EC, Baker NL, Morita M, Hamamoto H, Ryan LP, Gorman JH 3rd, Spinale FG. Targeted regional injection of biocomposite microspheres alters post-myocardial infarction remodeling and matrix proteolytic pathways. Circulation. 2011; 124:S35–45. [PubMed: 21911817]
8. Wilson EM, Moainie SL, Baskin JM, Lowry AS, Deschamps AM, Mukherjee R, Guy TS, St John-Sutton MG, Gorman JH 3rd, Edmunds LH Jr, Gorman RC, Spinale FG. Region- and type-specific induction of matrix metalloproteinases in post-myocardial infarction remodeling. Circulation. 2003; 107:2857–2863. [PubMed: 12771000]

9. Spinale FG, Janicki JS, Zile MR. Membrane-associated matrix proteolysis and heart failure. Circulation research. 2013; 112:195–208. [PubMed: 23287455]
10. Araszkiewicz A, Grajek S, Lesiak M, Prech M, Pyda M, Janus M, Cieslinski A. Effect of impaired myocardial reperfusion on left ventricular remodeling in patients with anterior wall acute myocardial infarction treated with primary coronary intervention. The American journal of cardiology. 2006; 98:725–728. [PubMed: 16950171]
11. Quijada P, Toko H, Fischer KM, Bailey B, Reilly P, Hunt KD, Gude NA, Avitabile D, Sussman MA. Preservation of myocardial structure is enhanced by pim-1 engineering of bone marrow cells. Circulation research. 2012; 111:77–86. [PubMed: 22619278]
12. Vrtovec B, Poglajen G, Lezaic L, Sever M, Domanovic D, Cernelc P, Socan A, Schrepfer S, Torre-Amione G, Haddad F, Wu JC. Effects of intracoronary cd34+ stem cell transplantation in nonischemic dilated cardiomyopathy patients: 5-year follow-up. Circulation research. 2013; 112:165–173. [PubMed: 23065358]
13. Houtgraaf JH, de Jong R, Kazemi K, de Groot D, van der Spoel TI, Arslan F, Hoefer I, Pasterkamp G, Itescu S, Zijlstra F, Geleijnse ML, Serruys PW, Duckers HJ. Intracoronary infusion of allogeneic mesenchymal precursor cells directly after experimental acute myocardial infarction reduces infarct size, abrogates adverse remodeling, and improves cardiac function. Circulation research. 2013; 113:153–166. [PubMed: 23658436]
14. Duran JM, Makarewich CA, Sharp TE, Starosta T, Zhu F, Hoffman NE, Chiba Y, Madesh M, Berretta RM, Kubo H, Houser SR. Bone-derived stem cells repair the heart after myocardial infarction through transdifferentiation and paracrine signaling mechanisms. Circulation research. 2013; 113:539–552. [PubMed: 23801066]
15. Askari AT, Unzek S, Popovic ZB, Goldman CK, Forudi F, Kiedrowski M, Rovner A, Ellis SG, Thomas JD, DiCorleto PE, Topol EJ, Penn MS. Effect of stromal-cell-derived factor 1 on stem-cell homing and tissue regeneration in ischaemic cardiomyopathy. Lancet. 2003; 362:697–703. [PubMed: 12957092]
16. Yamaguchi J, Kusano KF, Masuo O, Kawamoto A, Silver M, Murasawa S, Bosch-Marce M, Masuda H, Losordo DW, Isner JM, Asahara T. Stromal cell-derived factor-1 effects on ex vivo expanded endothelial progenitor cell recruitment for ischemic neovascularization. Circulation. 2003; 107:1322–1328. [PubMed: 12628955]
17. Escot S, Blavet C, Hartle S, Duband JL, Fournier-Thibault C. Misregulation of sdf1-cxcr4 signaling impairs early cardiac neural crest cell migration leading to conotruncal defects. Circulation research. 2013; 113:505–516. [PubMed: 23838132]
18. Dai S, Yuan F, Mu J, Li C, Chen N, Guo S, Kingery J, Prabhu SD, Bolli R, Rokosh G. Chronic amd3100 antagonism of sdf-1alpha-cxcr4 exacerbates cardiac dysfunction and remodeling after myocardial infarction. Journal of molecular and cellular cardiology. 2010; 49:587–597. [PubMed: 20655922]
19. Woo YJ, Grand TJ, Berry MF, Atluri P, Moise MA, Hsu VM, Cohen J, Fisher O, Burdick J, Taylor M, Zentko S, Liao G, Smith M, Kolakowski S, Jayasankar V, Gardner TJ, Sweeney HL. Stromal cell-derived factor and granulocyte-monocyte colony-stimulating factor form a combined neovasculogenic therapy for ischemic cardiomyopathy. The Journal of thoracic and cardiovascular surgery. 2005; 130:321–329. [PubMed: 16077394]
20. Zhang M, Mal N, Kiedrowski M, Chacko M, Askari AT, Popovic ZB, Koc ON, Penn MS. Sdf-1 expression by mesenchymal stem cells results in trophic support of cardiac myocytes after myocardial infarction. FASEB journal : official publication of the Federation of American Societies for Experimental Biology. 2007; 21:3197–3207. [PubMed: 17496162]
21. Unzek S, Zhang M, Mal N, Mills WR, Laurita KR, Penn MS. Sdf-1 recruits cardiac stem cell-like cells that depolarize in vivo. Cell transplantation. 2007; 16:879–886. [PubMed: 18293886]
22. Sundararaman S, Miller TJ, Pastore JM, Kiedrowski M, Aras R, Penn MS. Plasmid-based transient human stromal cell-derived factor-1 gene transfer improves cardiac function in chronic heart failure. Gene therapy. 2011; 18:867–873. [PubMed: 21472007]
23. Frederick JR, Fitzpatrick JR 3rd, McCormick RC, Harris DA, Kim AY, Muenzer JR, Marotta N, Smith MJ, Cohen JE, Hiesinger W, Atluri P, Woo YJ. Stromal cell-derived factor-1alpha activation of tissue-engineered endothelial progenitor cell matrix enhances ventricular function

after myocardial infarction by inducing neovasculogenesis. Circulation. 2010; 122:S107–117. [PubMed: 20837901]

24. Hu X, Dai S, Wu WJ, Tan W, Zhu X, Mu J, Guo Y, Bolli R, Rokosh G. Stromal cell derived factor-1 alpha confers protection against myocardial ischemia/reperfusion injury: Role of the cardiac stromal cell derived factor-1 alpha cxcr4 axis. Circulation. 2007; 116:654–663. [PubMed: 17646584]
25. Penn MS, Mendelsohn FO, Schaer GL, Sherman W, Farr M, Pastore J, Rouy D, Clemens R, Aras R, Losordo DW. An open-label dose escalation study to evaluate the safety of administration of nonviral stromal cell-derived factor-1 plasmid to treat symptomatic ischemic heart failure. Circulation research. 2013; 112:816–825. [PubMed: 23429605]
26. Hiesinger W, Frederick JR, Atluri P, McCormick RC, Marotta N, Muenzer JR, Woo YJ. Spliced stromal cell-derived factor-1alpha analog stimulates endothelial progenitor cell migration and improves cardiac function in a dose-dependent manner after myocardial infarction. The Journal of thoracic and cardiovascular surgery. 2010; 140:1174–1180. [PubMed: 20951261]
27. Hiesinger W, Perez-Aguilar JM, Atluri P, Marotta NA, Frederick JR, Fitzpatrick JR 3rd, McCormick RC, Muenzer JR, Yang EC, Levit RD, Yuan LJ, Macarthur JW, Saven JG, Woo YJ. Computational protein design to reengineer stromal cell-derived factor-1alpha generates an effective and translatable angiogenic polypeptide analog. Circulation. 2011; 124:S18–26. [PubMed: 21911811]
28. Hiesinger W, Brukman MJ, McCormick RC, Fitzpatrick JR 3rd, Frederick JR, Yang EC, Muenzer JR, Marotta NA, Berry MF, Atluri P, Woo YJ. Myocardial tissue elastic properties determined by atomic force microscopy after stromal cell-derived factor 1alpha angiogenic therapy for acute myocardial infarction in a murine model. The Journal of thoracic and cardiovascular surgery. 2012; 143:962–966. [PubMed: 22264415]
29. Hiesinger W, Goldstone AB, Woo YJ. Re-engineered stromal cell-derived factor-1alpha and the future of translatable angiogenic polypeptide design. Trends in cardiovascular medicine. 2012; 22:139–144. [PubMed: 22902182]
30. MacArthur JW Jr, Trubelja A, Shudo Y, Hsiao P, Fairman AS, Yang E, Hiesinger W, Sarver JJ, Atluri P, Woo YJ. Mathematically engineered stromal cell-derived factor-1alpha stem cell cytokine analog enhances mechanical properties of infarcted myocardium. The Journal of thoracic and cardiovascular surgery. 2013; 145:278–284. [PubMed: 23244259]
31. Macarthur JW Jr, Purcell BP, Shudo Y, Cohen JE, Fairman A, Trubelja A, Patel J, Hsiao P, Yang E, Lloyd K, Hiesinger W, Atluri P, Burdick JA, Woo YJ. Sustained release of engineered stromal cell-derived factor 1-alpha from injectable hydrogels effectively recruits endothelial progenitor cells and preserves ventricular function after myocardial infarction. Circulation. 2013; 128:S79–86. [PubMed: 24030424]
32. Markovitz LJ, Savage EB, Ratcliffe MB, Bavaria JE, Kreiner G, Iozzo RV, Hargrove WC 3rd, Bogen DK, Edmunds LH Jr. Large animal model of left ventricular aneurysm. The Annals of thoracic surgery. 1989; 48:838–845. [PubMed: 2596920]
33. Koomalsingh KJ, Witschey WR, McGarvey JR, Shuto T, Kondo N, Xu C, Jackson BM, Gorman JH 3rd, Gorman RC, Pilla JJ. Optimized local infarct restraint improves left ventricular function and limits remodeling. The Annals of thoracic surgery. 2013; 95:155–162. [PubMed: 23146279]
34. Yushkevich PA, Piven J, Hazlett HC, Smith RG, Ho S, Gee JC, Gerig G. User-guided 3d active contour segmentation of anatomical structures: Significantly improved efficiency and reliability. NeuroImage. 2006; 31:1116–1128. [PubMed: 16545965]
35. Xu C, Pilla JJ, Isaac G, Gorman JH 3rd, Blom AS, Gorman RC, Ling Z, Dougherty L. Deformation analysis of 3d tagged cardiac images using an optical flow method. Journal of cardiovascular magnetic resonance : official journal of the Society for Cardiovascular Magnetic Resonance. 2010; 12:19. [PubMed: 20353600]
36. Rentrop KP, Cohen M, Blanke H, Phillips RA. Changes in collateral channel filling immediately after controlled coronary artery occlusion by an angioplasty balloon in human subjects. Journal of the American College of Cardiology. 1985; 5:587–592. [PubMed: 3156171]
37. Blom AS, Pilla JJ, Arkles J, Dougherty L, Ryan LP, Gorman JH 3rd, Acker MA, Gorman RC. Ventricular restraint prevents infarct expansion and improves borderzone function after myocardial infarction: A study using magnetic resonance imaging, three-dimensional surface

modeling, and myocardial tagging. The Annals of thoracic surgery. 2007; 84:2004–2010. [PubMed: 18036925]

38. Morita M, Eckert CE, Matsuzaki K, Noma M, Ryan LP, Burdick JA, Jackson BM, Gorman JH 3rd, Sacks MS, Gorman RC. Modification of infarct material properties limits adverse ventricular remodeling. The Annals of thoracic surgery. 2011; 92:617–624. [PubMed: 21801916]
39. Janowska-Wieczorek A, Marquez LA, Dobrowsky A, Ratajczak MZ, Cabuhat ML. Differential mmp and timp production by human marrow and peripheral blood cd34(+) cells in response to chemokines. Experimental hematology. 2000; 28:1274–1285. [PubMed: 11063876]
40. Uchinaka A, Kawaguchi N, Hamada Y, Miyagawa S, Saito A, Mori S, Sawa Y, Matsuura N. Transplantation of elastin-secreting myoblast sheets improves cardiac function in infarcted rat heart. Molecular and cellular biochemistry. 2012; 368:203–214. [PubMed: 22718481]
41. Li SH, Sun Z, Guo L, Han M, Wood MF, Ghosh N, Vitkin IA, Weisel RD, Li RK. Elastin overexpression by cell-based gene therapy preserves matrix and prevents cardiac dilation. Journal of cellular and molecular medicine. 2012; 16:2429–2439. [PubMed: 22435995]

## Nonstandard Abbreviations and Acronyms

| | |
|---|---|
| **ECM** | Extracellular matrix |
| **EDV** | end diastolic volume |
| **EF** | ejection fraction |
| **EPC** | endothelial progenitor cell |
| **ESA** | engineered stromal cell-derived factor 1-α analogue |
| **ESV** | End systolic volume |
| **IVC** | inferior vena cava |
| **LGE** | late gadolinium enhancement |
| **MI** | myocardial infarction |
| **MMP** | matrix metalloproteinase |
| **PV** | pressure volume |
| **SDF-1** | stromal cell-derived factor 1-α |
| **SPAMM** | spatial modulation of magnetization |
| **SSFP** | steady state free precession |
| **SV** | stroke volume |
| **TIMP** | tissue inhibitor of matrix metalloproteinase |

## Novelty and Significance

**What Is Known?**

- Delivery of bone marrow progenitor cells after a myocardial infarction (MI) improves ventricular function.
- Stromal cell-derived factor 1-alpha (SDF-1) mobilizes endothelial progenitor cells (EPCs) from the bone marrow to areas of myocardial ischemia; however cardiac secretion of SDF-1 is insufficiently robust to mobilize a sufficient number of EPCs to affect meaningful changes in perfusion.
- SDF-1 is broken down by multiple peptidases and recombinant production is inefficient and expensive.

**What New Information Does this Article Contribute?**

- Using computational modeling, a biomolecularly-designed version of SDF-1 was created to overcome the limitations of the recombinant protein.
- Engineered SDF- 1-alpha analogue (ESA) effectively recruits EPCs.
- Intramyocardial delivery of ESA in a preclinical, large animal acute MI model, leads to increased myocardial perfusion, smaller infarcts, improved borderzone contractility, and limited ventricular remodeling.

After an MI, the resulting deficit in microvascular perfusion ultimately leads to myocyte apoptosis, infarct spreading, ventricular dilatation, and heart failure. Localization of EPCs to the border zone of the infarct preserves myocardial perfusion and limits myocardial injury. Cardiac secretion of SDF-1 is unable to recruit a sufficient number of EPCs to achieve improved perfusion. We hypothesized that ESA delivery to the infarct border zone would induce EPC chemotaxis, improve myocardial perfusion, limit ventricular remodeling, and improve borderzone contractility. We found clear EPC chemotaxis across an ESA gradient and significant regional functional improvements in ventricular function in a large animal, acute MI model. This improvement in function appears to be due to micro-revascularization by ESA treatment, resulting in reduced ventricular remodeling. Together, these findings provide support for the translational use of ESA in human subjects with acute MI in an effort to prevent the progression to ischemic cardiomyopathy.

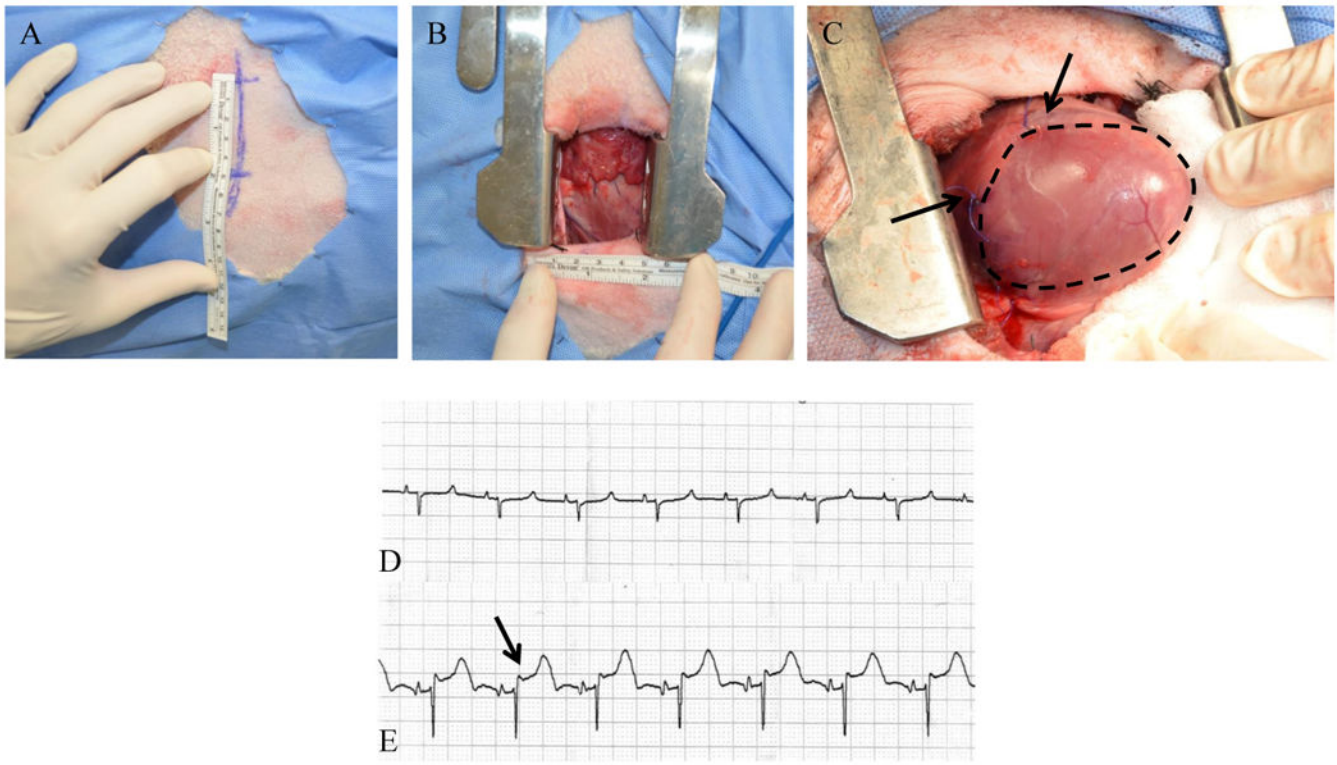


**Figure 1. Operative Exposure and Induction of MI**

A left anterior, 5 cm minithoracotomy was used to enter the chest and expose the heart (A, B). **C**, The LAD and D2 branches were ligated with polypropylene suture, creating an anteroapical infarct (black arrows denote site of suture ligation, infarct outlined in black). Pre (**D**) and post (**E**) ligation ECGs were recorded and printed. ST segment elevation (black arrow in panel **E**) confirmed transmural infarction in all animals.

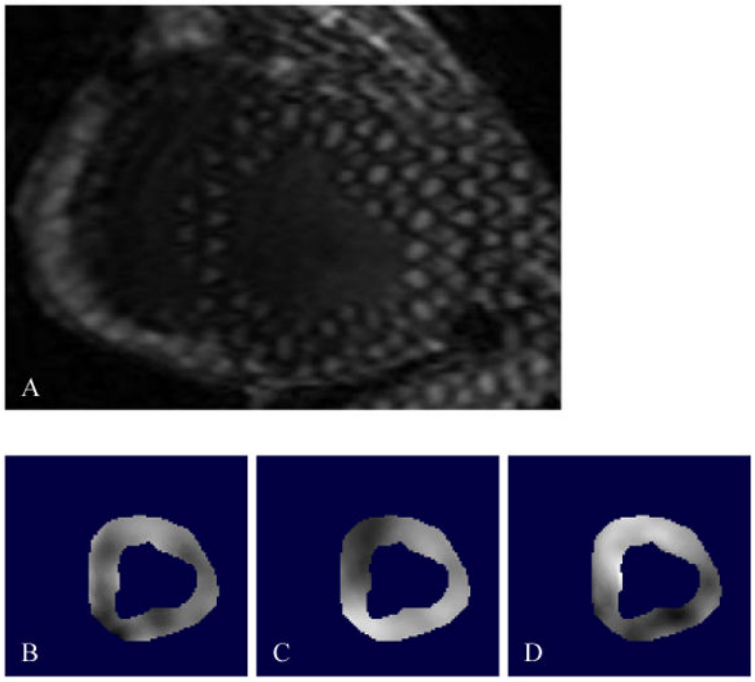


**Figure 2. 3D SPAMM Acquisition and the Optical Flow Technique**

**A**, SPAMM creates a periodic modulation of magnetization along a desired direction by applying a series of non-selective excitation pulses, creating tagged lines that move with the myocardium, providing a 3D sample of cardiac motion. This is a representative cross sectional 3D SPAMM tagged image of the LV, where three tag planes are utilized; two through plane tags and one oblique tag plane. Blood appears black and the myocardium is bright. In order to measure systolic regional strain, the LV myocardium was contoured to create an image mask and a custom optical flow plug-in for Image J was used to calculate x, y, and z displacement flow fields (**B**,**C**, and **D**, respectively).

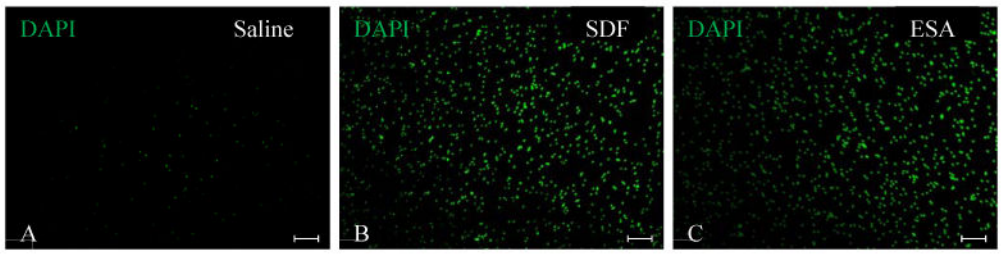


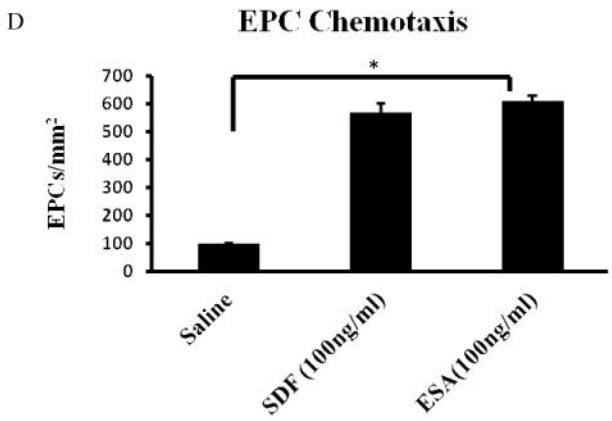


**Figure 3. Transwell Migration Assay**

**A**, Representative images of modified transwell Boyden chamber migration assay filters demonstrating EPC migration in saline, SDF, and ESA gradients. (B) The graph summarizes EPC migration between groups. *$p<0.05$, scale bar = 75μm.

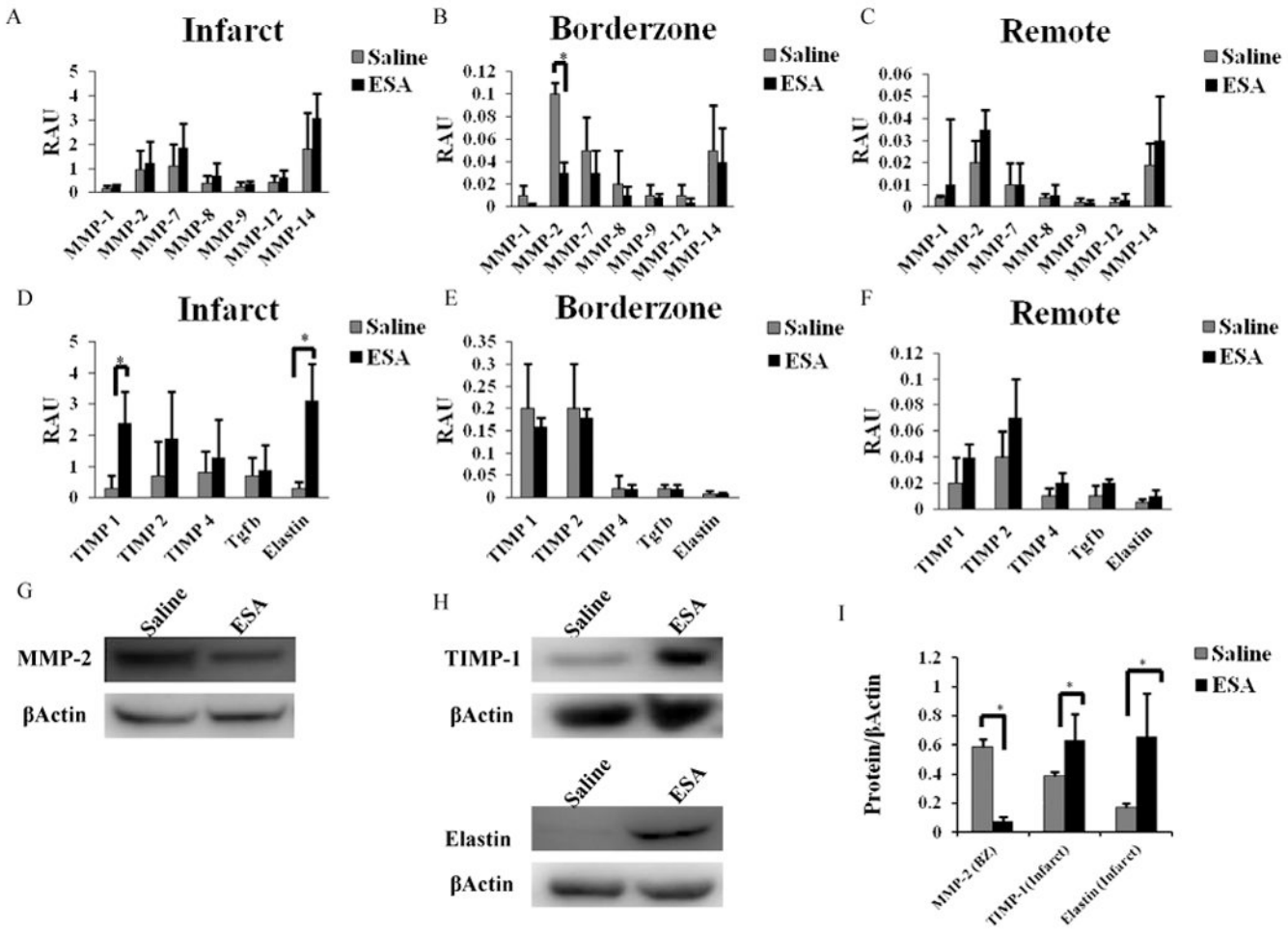


**Figure 4. LV mRNA and Protein Expression Profile**

**A-F**, mRNA analysis of MMP, TIMP, elastin and transforming growth factor beta (Tgfb) were performed on myocardial biopsies from infarct, borderzone, and remote areas of the LV. Samples were standardized to mRNA of GAPDH (RFU = ratio of fluorescence units). (**B**) MMP-2 levels are decreased in the borderzone of ESA treated animals and (**D**) TIMP-1 and elastin levels are increased in the infarct of ESA treated animals. In order to confirm that protein expression correlated to the observed mRNA expression, immunoblots were performed on myocardial biopsies from infarct, borderzone, and remote areas of the LV. Representative immunoblots show (**G**) decreased expression of MMP-2 in the borderzone and (**H**) increased expression of TIMP-1 and elastin in the infarct region of ESA treated animals compared to those treated with saline. **I**, Values are presented as a ratio of β-actin expression. *p<0.05, BZ = borderzone.

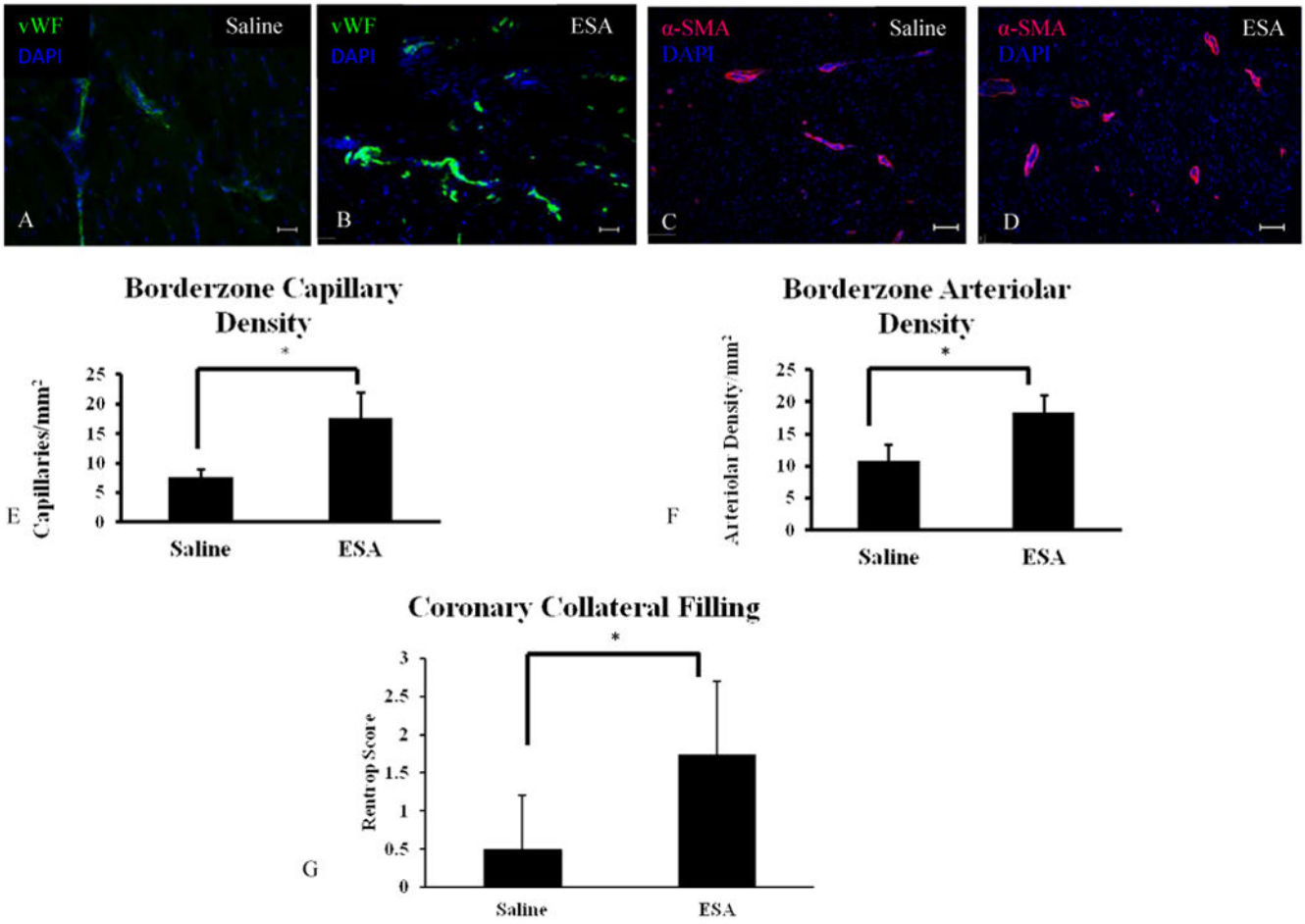


**Figure 5. Vascular Density and Myocardial Perfusion**

Immunohistochemical light microscope images of borderzone myocardium using anti-vWF antibody (**A-B**) and anti-αSMA antibody (**C-D**). Analysis of immunofluorescent expression of vWF and αSMA revealed a significant increase in signal in the ESA group compared to saline (**E-F**, respectively). Coronary angiograms were reviewed and assessed for collateral filling using Rentrop scores in an effort to evaluate whether or not the increased vascularity seen from the immunohistochemical data resulted in increased myocardial perfusion. **G**, Coronary angiograms from animals in the ESA group had significantly higher Rentrop scores, and hence better collateral filling, compared to angiograms from animals in the saline group. *$p<0.05$, scale bar = 75μm.

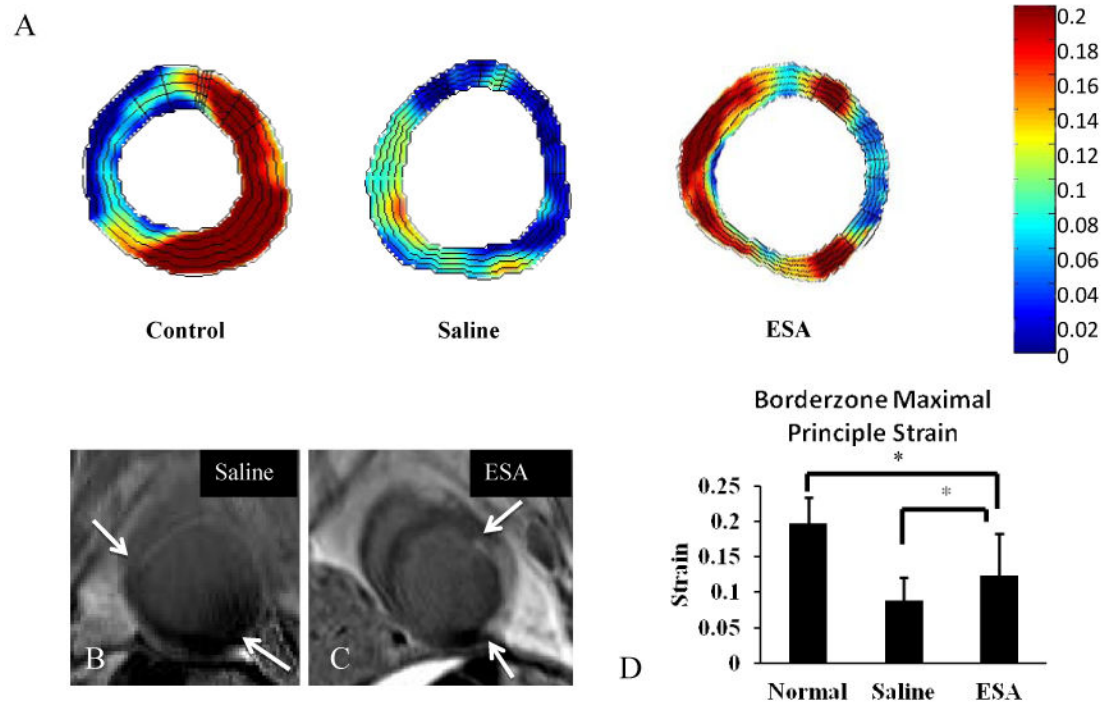


**Figure 6. Maximal Principle Strain Analysis**

**A**, Color map of regional maximum principle strain from cross sections of the LV. Representative color maps of hearts from ESA treated animals show elevated (red on color map) regional strain about the borderzone. Hearts from saline treated animals show decreased (green to blue) regional strain about the borderzone. Representative color map of a heart from a normal animal without MI shows a characteristic strain pattern with elevated strain throughout the free wall of the LV. **B**, Cross sectional late gadolinium enhanced MRI images corresponding to the strain maps from the saline and ESA groups (white arrows delineate boundary of infarct; scar tissue shows up white from gadolinium contrast). **C**, Regional strain at the borderzone is significantly elevated in hearts from animals treated with ESA compared to hearts from animals treated with saline, and closer to healthy myocardium. *$p<0.05$.

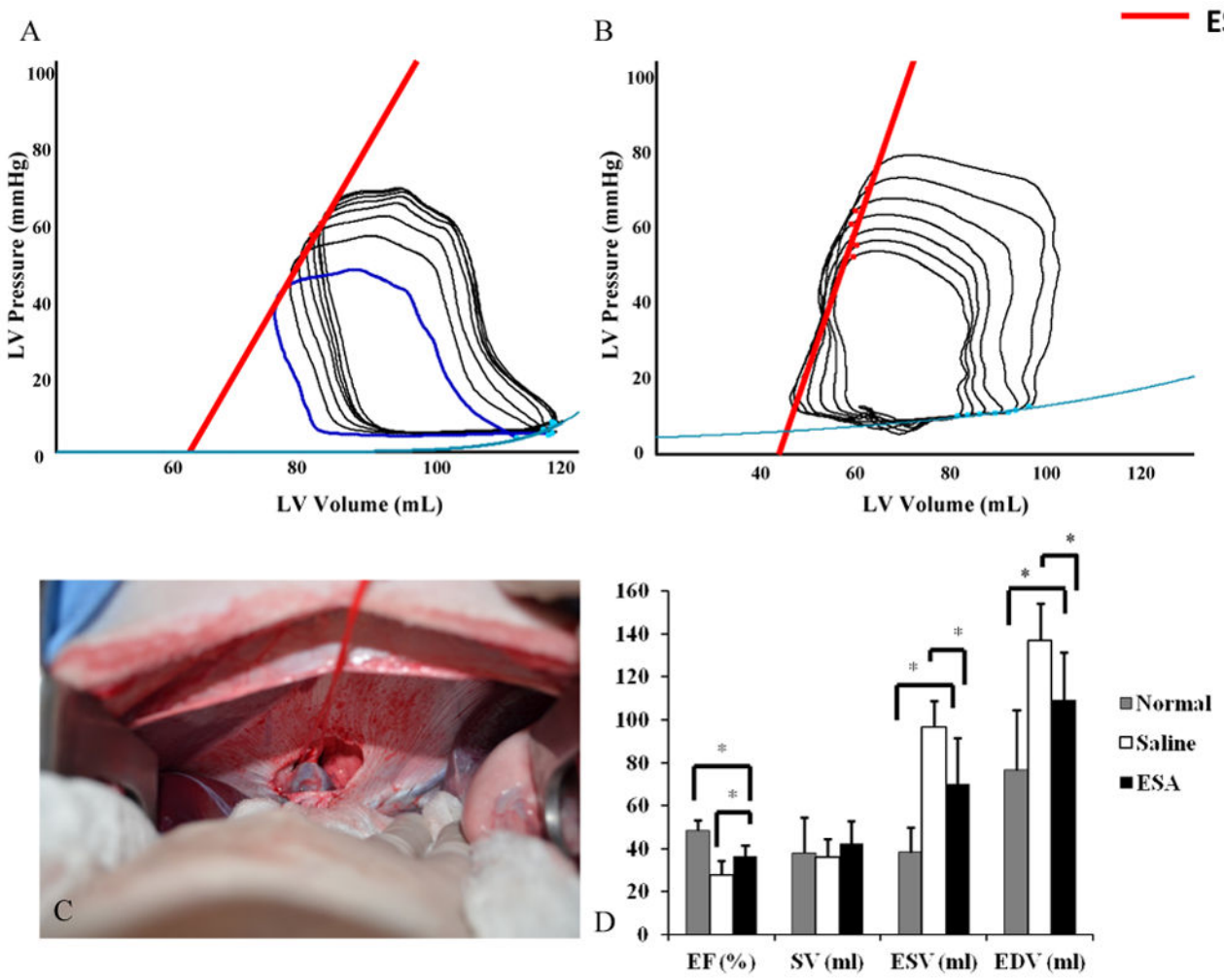


**Figure 7. Hemodynamic Assessment**

Pressure-volume loops were obtained during IVC occlusion for variable load data. (**A-B**) Representative PV loops from animals in the saline group and ESA group. Note the increased slope of the ESPVR (red line) in the ESA group, a pre-load independent measure of myocardial contractility. **C**, Before PV loop acquisition, a small upper midline laparotomy was performed and the suprahepatic IVC was dissected free and encircled with a vessel loop. This is a representative image of complete IVC occlusion by gentle retraction on the vessel loop. **D**, Animals in the ESA group had improved EF, lower ESV, and lower EDV compared to animals in the saline group, representing preserved LV function and limited LV remodeling. *p<0.05. EF = ejection fraction, SV = stroke volume, ESV = end systolic volume, EDV = end diastolic volume.

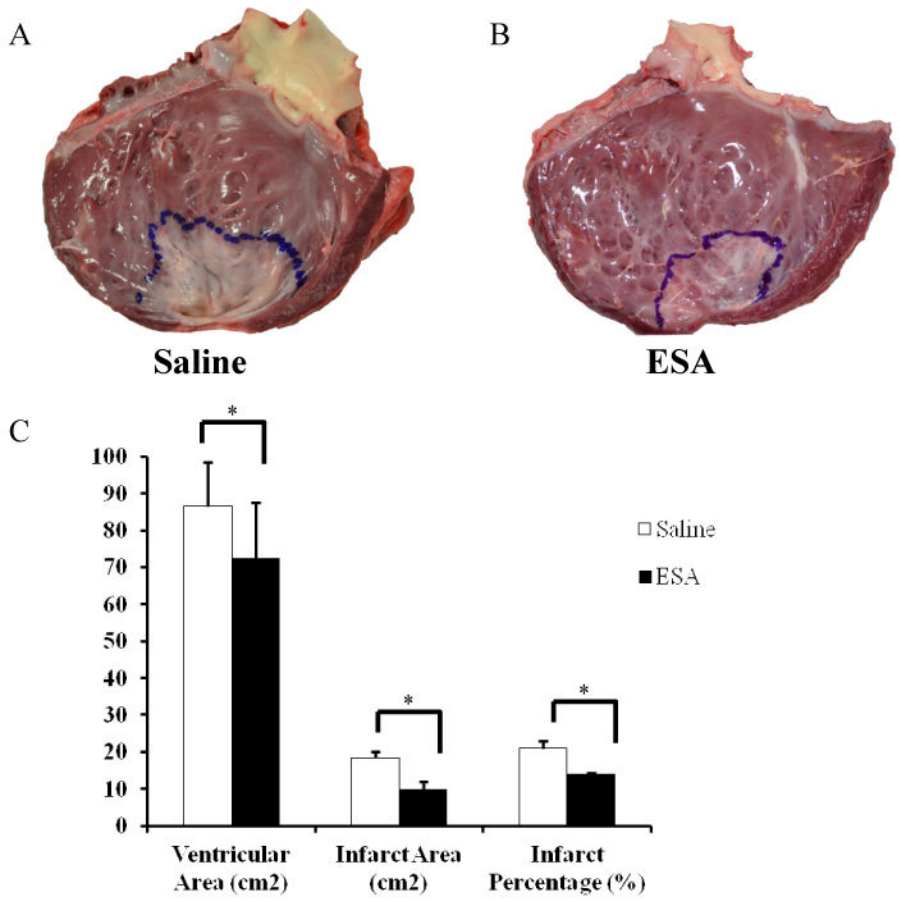


**Figure 8. LV Infarct Area**

Hearts were explanted and opened longitudinally. The infarct was outlined and photographed for quantification. Representative images of a heart from an animal in the saline group (**A**) and a heart from an animal in the ESA treated group (**B**). **C**, Animals in the ESA group had significantly reduced surface area of the LV and smaller infarct sizes when compared to animals in the saline group. *p<0.05.